IEEE Access
Multidisciplinary ⋮ Rapid Review ⋮ Open Access Journal

Received 24 February 2026, accepted 6 March 2026, date of publication 23 March 2026, date of current version 26 March 2026.

Digital Object Identifier 10.1109/ACCESS.2026.3676071

RESEARCH ARTICLE

Leg-Shared System Integrating Grid-Connected Photovoltaic and Dynamic Wireless Power Transfer

NOZOMI MURAYAMA, (Student Member, IEEE), TAKEHIRO IMURA, (Member, IEEE), AND YOICHI HORI

Department of Electrical Engineering, Faculty of Science and Technology, Tokyo University of Science, Noda 162-8601, Japan

Corresponding author: Nozomi Murayama (murayama.nozomi23@gmail.com)

ABSTRACT By combining dynamic wireless power transfer (DWPT) for charging electric vehicles (EVs) with the miniaturization of onboard batteries, it is possible to reduce the size of onboard batteries and extend their driving range, thereby suppressing CO_2 emissions generated during EV manufacturing. Furthermore, sourcing the power supply for EVs from photovoltaics (PV) can significantly contribute to achieving carbon neutrality. This paper proposes a PV+DWPT system combining a grid-connected PV system with a DWPT system. However, challenges remain, such as the DWPT system being usable only while the vehicle is in motion, and the power grid having to adjust to the fluctuating power from the PV. Therefore, the proposed system improves the overall circuit utilization rate by sharing the legs of the DC–DC Converter used for PV and the Full-Bridge Inverter used for DWPT. Furthermore, it reduces the burden on the power grid by using an Electric Double-Layer Capacitor (EDLC). The proposed system was verified through a bench-scale experiment using three transmitting coils and one receiving coil. The results demonstrate a maximum power point tracking (MPPT) efficiency of 85.2% under fluctuating irradiance and a DWPT transmission efficiency of 81.2%. These findings confirm the effectiveness of the proposed system in ensuring a stable power supply and reducing grid impact, thereby demonstrating its potential for sustainable transportation infrastructure.

INDEX TERMS Bench-scale experiment, dynamic wireless power transfer, electric double-layer capacitor, leg-shared, maximum power point tracking, photovoltaic, receiving coil, transmitting coil.

I. INTRODUCTION

A. INSPIRATION AND MOTIVATION

In recent years, the global push toward a decarbonized society has accelerated the adoption of electric vehicles (EVs). However, current EVs face structural challenges: lengthy charging processes, limited driving range, reduced energy efficiency due to battery weight, and significant carbon dioxide emissions during battery manufacturing. As a solution, Dynamic Wireless Power Transfer (DWPT), which transmits power to EVs while they are in motion, is gaining attention. This system not only simultaneously achieves extended range and vehicle weight reduction but also enables a reduction in the environmental impact during EV manufacturing. Consequently, DWPT is being actively researched by institutions both domestically and internationally as an innovative technology contributing to carbon neutrality [1], [2], [3], [4], [5], [6], [7], [8], [9], [10], [11].

While EV adoption directly reduces greenhouse gas emissions during operation, further supply of driving energy from renewable sources can significantly contribute to achieving carbon neutrality. Solar power, also known as photovoltaics (PV), is widely recognized as one of the most accessible and widely adopted renewable energy sources. Nevertheless, the large-scale deployment of PV systems requires countermeasures against the duck curve phenomenon, which arises from the mismatch between power supply and demand. This involves a sharp decrease in net load during the day, followed by a surge in the evening. DWPT systems provide significant synergy here, as their daytime power

The associate editor coordinating the review of this manuscript and approving it for publication was Youngjin Kim.

requirements coincide with the peak generation hours of PV systems. Against this backdrop, developing a PV+DWPT system that integrates PV and DWPT is a critically important consideration. This paper proposes a grid-connected PV+DWPT system utilizing the power grid and PV as power sources. The primary purpose of connecting to the power grid is to adjust for surplus and deficit power caused by fluctuations in PV output, ensuring a stable power supply to the DWPT system. Therefore, this study is particularly motivated by the inherent synergy between the peak generation hours of PV systems and the daytime power requirements of DWPT.

B. LITERATURE REVIEW

Various architectures for PV-integrated DWPT systems have been explored to balance renewable energy utilization and grid stability [12], [13], [14], [15], [16], [17], [18], [19]. Early modular approaches focused on system-level stabilization using external energy storage or grid-connected interfaces. For instance, Sugizaki et al. [16] proposed an off-grid system incorporating battery energy storage (BESS), while Urano et al. [18] demonstrated a grid-connected architecture that stabilized the DC bus using independent converters.

Building on these concepts, our prior work [19] implemented a system using a Dual Active Bridge (DAB) converter to regulate power between the grid and the DC bus. However, as noted in [19], several issues remained, including high semiconductor counts and a significant reliance on the grid for absorbing surplus PV power. While these previous studies [16], [18], [19] successfully established the fundamental feasibility of PV+DWPT, they relied on decoupled, modular converter stages. This study represents a significant progression from these modular approaches by advancing the integration to the circuit level through a leg-shared configuration. By integrating the power stages into a single unit, this paper achieves higher hardware density and a more unified control strategy, addressing the limitations of component redundancy and complex grid interactions identified in earlier works.

C. CONTRIBUTION AND PAPER ORGANIZATION

This paper proposes a leg-shared PV+DWPT topology to overcome the limitations of conventional systems. The proposed system integrates the PV boost DC–DC converter and the DWPT full-bridge inverter through a leg-shared configuration. This integrated architecture significantly reduces the total number of power components. Furthermore, this integration enables a simplified integrated control strategy to effectively mitigate the impact on the power grid. The main contributions of this study, which directly address the technical requirements for practical deployment, are as follows:

1. Hardware Integration (Architectural Novelty): Development of an integrated topology combining the PV and DWPT systems that reduces the number of switching elements in the power conversion stage by 33.3% (from 6 to 4 MOSFETs) compared to conventional decoupled architectures.
2. Simplified Integrated Control (Control Novelty): Implementation of a unified mode-switching control integrated with an EDLC-based buffer. This simplified strategy ensures DC bus stability within 0.93% of the rated voltage, providing quantitative evidence that the power grid is shielded from high-frequency power spikes even during rapid vehicle transitions.
3. Experimental Validation based on Real-world Data: Evaluation of the system's robustness through a bench-scale experiment. By utilizing the actual traffic data analyzed in Section III and applying aggressive time compression, this study proves that the proposed integrated control can reliably manage power fluctuations under demanding, real-world-inspired conditions.

The remainder of this paper is organized as follows: Section II describes the proposed system configuration and its operation modes; Section III presents the power requirement estimation based on real-world traffic data; Section IV discusses the experimental setup and results; and finally, Section V concludes the paper.

II. PROPOSED SYSTEM CONFIGURATION

This section discusses the challenges of conventional grid-connected PV+DWPT systems and describes the proposed leg-shared PV+DWPT system and its configuration.

A. CONVENTIONAL PV+DWPT SYSTEM

We detail the issues identified in the prior research [19]. This paper uses a DAB converter to absorb all PV output fluctuations and DWPT's steep load variations on the power grid side. This significantly increases the grid's adjustment burden and leads to local voltage fluctuations and degraded power quality. Furthermore, under continuous operation, the DWPT subsystem inherently experiences prolonged periods of zero power demand depending on traffic volume and vehicle presence. During these inactive periods, the fact that the DWPT circuitry is not utilized for its primary purpose of power transmission significantly reduces the overall equipment utilization rate of the system. This is an extremely critical issue from the perspective of economic rationality and cost performance relative to the initial investment.

B. PROPOSED PV+DWPT SYSTEM

This study proposes a stable, leg-shared PV+DWPT system that resolves the problems described in the previous subsection. Specifically, the DC bus is implemented using EDLC, which acts as a central energy buffer between the PV and DWPT systems. Furthermore, by partially sharing the legs of the PV system's DC–DC converter and the DWPT system's full-bridge inverter, the system suppresses sudden power fluctuations, improves overall circuit utilization, and achieves stable operation. Here, a stable system refers to one with high robustness, capable of simultaneously maintaining maximum PV output and constant reception despite

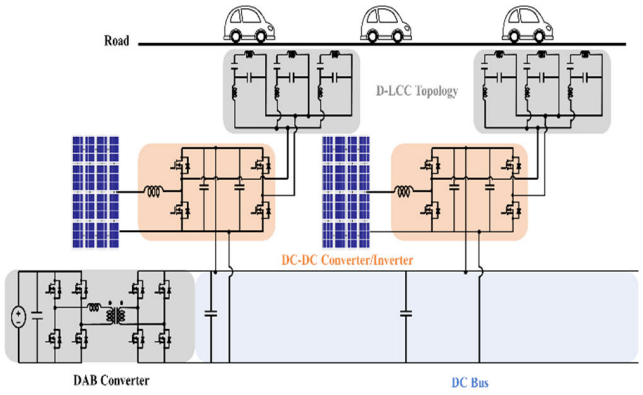

FIGURE 1. Overall view of the proposed PV+DWPT system, which integrates PV and DWPT via a leg-shared converter. The configuration includes a grid-connected DAB converter for power regulation and a Double-LCC topology for efficient wireless power delivery.

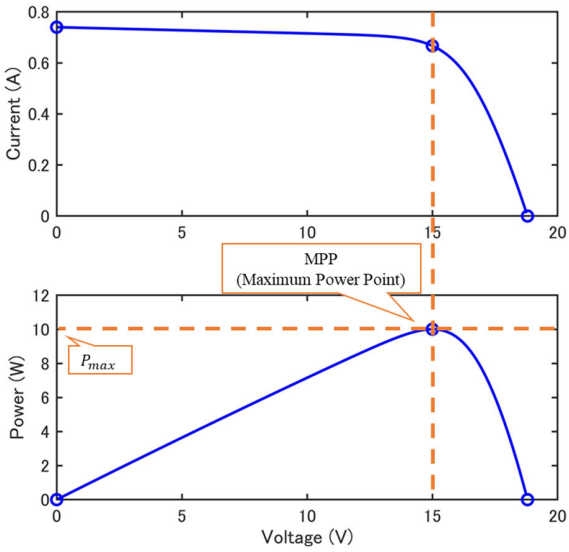

FIGURE 2. Illustrates the I-V and P-V characteristic curves of the solar panel used in the experiments. These curves provide the fundamental reference for evaluating the tracking accuracy and efficiency of the MPPT control algorithm during the bench-scale tests.

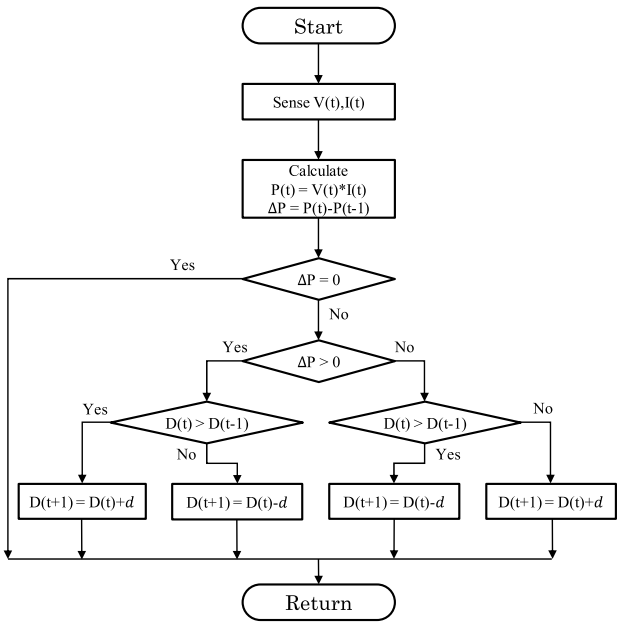

FIGURE 3. Illustrates the MPPT control flowchart using the P&O strategy. The algorithm iteratively adjusts the duty ratio based on power variations ⊿P to maximize PV output during standby mode.

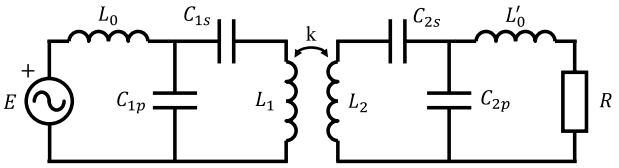

FIGURE 4. Double-sided LCC compensation topology. This configuration is designed to achieve high efficiency and constant current characteristics, with parameters optimized to maintain stable power delivery across the inductive coupling *k*.

disturbances such as changing weather conditions or mode transitions caused by vehicle entry.

Fig. 1 shows the overall view of the proposed system. The proposed system envisions a scenario where solar panels are installed near a highway performing DWPT, directly supplying power to the DWPT system. The PV output is regulated through maximum power point tracking (MPPT) via a DC–DC converter and delivered to the DC bus. The inverter outputs a square wave at 85 kHz and employs a Double-LCC circuit as the Wireless Power Transfer (WPT) compensation topology. A bidirectional DC–DC converter uses a DAB converter to perform constant voltage control of the DC bus. Details of each component are described in the upcoming subsections.

C. MPPT CONTROL WITH DC–DC CONVERTER

In the proposed system, the PV output power is regulated through MPPT via a DC–DC converter. MPPT control automatically tracks the optimal voltage and current values that maximize power output during solar cell operation. While several MPPT methods exist, this paper employs the Perturbation and Observation method (P&O method) [20], [21], [22], a classical approach that is simple to implement. As shown in Fig. 2, the output power of a solar cell varies with its output voltage. Therefore, a maximum power point exists where the solar cell's output is maximized. The P&O method continuously changes the voltage in one direction (increasing or decreasing). When the power changes direction, the voltage change direction is reversed. Repeating this process controls the system to the maximum power point. The flowchart of the P&O method used in the proposed system is shown in Fig. 3.

D. DOUBLE-LCC CIRCUIT FOR DWPT

The proposed DWPT system employs a double-LCC circuit as its compensation topology [23], [24], [25], [26], as illustrated in Fig. 4. This resonant network is designed to achieve LC resonance within each closed loop, with the inductance and capacitance values satisfying the resonance condition

defined by (1).

$$f_0 = \frac{1}{2\pi\sqrt{L_0 C_{1p}}} = \frac{1}{2\pi}\sqrt{\frac{C_{1p}+C_{1s}}{L_1 C_{1p} C_{1s}}} = \frac{1}{2\pi\sqrt{L_0' C_{2p}}} = \frac{1}{2\pi}\sqrt{\frac{C_{2p}+C_{2s}}{L_2 C_{2p} C_{2s}}} \quad (1)$$

A significant advantage of the double-LCC topology is its inherent load-sensing capability. When a receiving coil is magnetically coupled with a transmitting coil, power is efficiently transferred from source E. Conversely, in the absence of a receiver (i.e., when the coupling coefficient $k = 0$), the primary-side resonant network exhibits high input impedance, which inherently suppresses the current draw from the inverter. This characteristic allows the inverter output to adapt passively to vehicle traffic, enabling effective power management without complex external switching control, even when multiple transmitting coils are connected to a single inverter. Consequently, the adoption of the double-LCC circuit minimizes standby losses and simplifies the overall control architecture of the proposed system.

E. EDLC FOR POWER BUFFERING

The DC bus in this architecture essentially consists of an EDLC. The EDLC acts as a power buffer to mitigate fluctuations in PV output and abrupt load variations inherent to DWPT operations. The critical requirements for such a power buffer include the durability to withstand frequent, high-intensity charge/discharge cycles and the capability for rapid energy storage and release. EDLCs are uniquely suited to these demands as they exhibit negligible degradation even after hundreds of thousands to millions of cycles, while supporting high-rate charging and discharging. Consequently, EDLCs are integrated into the proposed configuration to ensure stable and responsive power management.

F. CONSTANT VOLTAGE CONTROL WITH DAB CONVERTER

A DAB converter is employed as the bidirectional DC–DC converter to interface the power grid with the DC bus, which is implemented using an EDLC. The DAB topology is selected for its ability to achieve high power density, facilitate zero-voltage switching (ZVS), and provide high power transmission efficiency. In this architecture, the primary role of the DAB converter is to maintain a constant voltage on the DC bus. The circuit configuration of the DAB converter is illustrated in Fig. 5.

To ensure stable operation, the DAB converter utilizes a proportional-integral (PI) controller as summarized in Fig. 6, referencing a conventional control strategy [27]. In this study, V_{in} corresponds to the grid voltage, while V_{out} is regulated. Crucially, rather than maintaining a rigid constant voltage, the DAB converter performs flexible regulation to allow the DC bus voltage to fluctuate within a predefined operational range. This strategy is essential for the EDLC-based DC bus to effectively function as a power buffer; by allowing

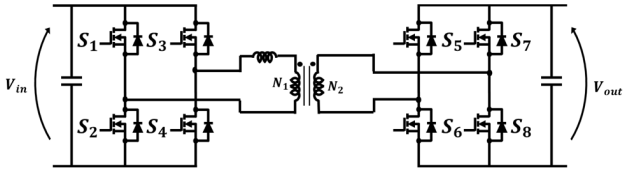

FIGURE 5. Illustrates the Dual Active Bridge (DAB) converter topology, which consists of two H-bridge stages isolated by a high-frequency transformer with an integrated leakage inductor.

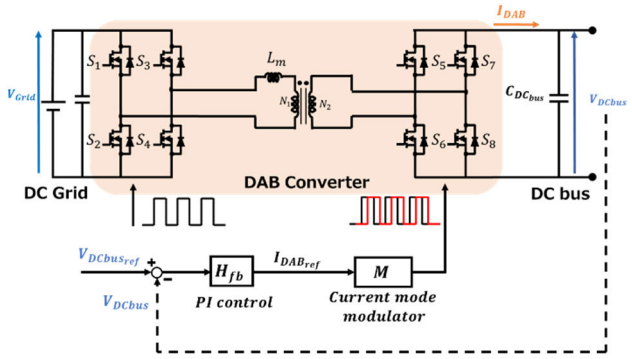

FIGURE 6. Presents the architecture and control logic of the DAB converter used for energy management between the DC grid and the DC bus. To maintain system stability, a closed-loop control system utilizes a PI controller and a current mode modulator to regulate the bus voltage according to its reference value.

controlled voltage variations, the EDLC can absorb or release energy to mitigate transient power mismatches between the PV generation and DWPT demand.

G. LEG-SHARED CIRCUIT CONFIGURATION AND OPERATIONAL MODES

The proposed system features a novel leg-shared circuit topology that integrates the PV boost DC–DC converter and the DWPT full-bridge inverter. By partially sharing power legs, the architecture enhances hardware utilization and facilitates device miniaturization. The operational modes and the functional roles of these shared legs are summarized in Table 1.

In the standby state (Mode 0), which occurs when no vehicle is detected, the shared legs function as a boost converter for the PV system. In this mode, the system performs MPPT control to maximize solar power extraction. Upon vehicle entry, the detection system triggers an instantaneous transition to the power supply state (Mode 1). In this mode, the functionality of the shared legs shifts to serve as part of the full-bridge inverter for the DWPT system. Power is then transmitted to the vehicle via phase-shift control while maintaining a constant duty ratio to ensure the delivery of maximum power. Once the vehicle's exit is detected, the system reverts to the standby state.

The coordinated action of the EDLC-based buffer and the unified control strategy ensures the transient stability during these transitions. During the shift from MPPT control to phase-shift control, the EDLC effectively absorbs any

TABLE 1. Shared leg operation modes.

OPERATION MODE	VEHICLE STATUS	SHARED LEG FUNCTION	CONTROL CONTENT
Standby (Mode 0)	No vehicle	DC–DC converter	MPPT control
Detection	Vehicle entering	Function switching	Entry detection
Power Supply (Mode 1)	Under charging	Full-bridge inverter	Phase-shift control
Detection	Vehicle passing	Function switching	Departure detection

TABLE 2. Comparison between the conventional system and the proposed Leg-shared system.

Parameters	Conventional System[19]	Proposed Leg-shared System
Circuit Components	Isolated Boost Converter + Inverter	Leg-shared PV + DWPT Converter
Number of MOSFETs	6	4
Hardware Reduction	-	33.3%
Control Architecture	Independent Control	Unified Integrated Control

instantaneous power mismatch, preventing unstable voltage oscillations on the DC bus. This control law ensures that the system maintains robustness even during rapid function switching of the shared legs.

By assigning dual functionality—acting as both a converter and an inverter—to the shared legs and synchronizing mode transitions with vehicle movement, the proposed system achieves significant circuit minimization. Furthermore, this approach enables flexible power management that is highly adaptable to varying weather conditions and vehicle demands.

To provide a quantitative assessment of these architectural benefits, Table 2 summarizes a comparison between the conventional system and the proposed leg-shared system. By integrating the PV boost DC–DC converter and the DWPT full-bridge inverter, the system reduces the switching element count by 33.3% (from 6 to 4 MOSFETs). This confirms the effectiveness of the proposed configuration in achieving hardware miniaturization.

III. POWER REQUIREMENT ESTIMATION BASED ON REAL-WORLD SCENARIOS

This section presents a power demand estimate derived from traffic data from the Ministry of Land, Infrastructure, Transport, and Tourism (MLIT) in Japan, to simulate the proposed system's implementation in practical settings. Based on these projections, the evaluation metrics for the bench-scale experiments in the following subsections are defined.

A. TRAFFIC DATA ANALYSIS AND MODELING CONDITIONS

The target area for this analysis is a 1-km segment of the Tomei Highway between the Ebina Junction and the Atsugi Interchange, a section characterized by some of the highest traffic volumes in Japan. Based on the Road Traffic Census data provided by MLIT, the 24-hour traffic volume N_{traffic} for this section is recorded at 70,791 vehicles. For the power demand estimation, this study assumes a future scenario in which EVs replace all internal combustion engine vehicles. To simplify the calculation conditions, no distinction is made between vehicle classes (e.g., heavy-duty vs. light-duty); instead, all vehicles are modeled as standard passenger EVs, specifically utilizing the specifications of the Nissan Leaf 62-kWh model with an energy consumption of 135 Wh/km.

B. CALCULATION OF REQUIRED ENERGY AND AVERAGE POWER SUPPLY

Based on these modeling conditions, the power requirements are defined at two distinct scales: the macro-level system capacity and the micro-level vehicle demand. The target energy supply per kilometer E_{target} is determined based on the energy consumption of the reference EV (135Wh/km) and the target coverage ratio of 80% as follows

$$E_{target} = 135 \times 0.8 \approx 0.11 \left[kWh/km\right] \tag{2}$$

At the macro level, the total daily energy demand E_{total} for the 1-km segment is calculated using $N_{traffic}$.

$$E_{total} = N_{traffic} \times E_{target} \approx 7787 \left[kWh/day\right] \tag{3}$$

To ensure the system can support this demand, the required continuous average power supply capacity P_{avg} can be obtained as

$$P_{avg} = \frac{E_{total}}{24[h]} \approx 324.5\,[kW] \tag{4}$$

At the micro level, the instantaneous power requirement for an individual vehicle P_{veh}, must be determined to ensure effective energy delivery during its passage. Given the average vehicle speed v, which is 51.4km/h according to MLIT, P_{veh} is calculated as

$$P_{veh} = E_{target} \times v \approx 5.65[kW] \tag{5}$$

For the bench-scale verification in this study, the micro-level requirement P_{veh} of 5.65 kW was scaled down by a factor of approximately 1/500 to a target received power of approximately 10 W due to laboratory equipment constraints. This scaling allows for a safe and detailed evaluation of the system's core control logic, including the MPPT-DWPT mode transitions and the buffering performance of the EDLC. The experimental results, which demonstrate that stable power delivery is maintained near this 10 W target throughout a simulated 24-hour cycle, serve as a fundamental proof-of-concept for the proposed system's ability to meet real-world power demands.

C. PV FLUCTUATION AND POWER SUPPLY CHALLENGES

The previous estimations clarify the baseline power requirements for the highway infrastructure. However, PV generation fluctuates significantly depending on meteorological conditions, making it challenging to maintain a constant power supply to the DWPT system. For practical implementation, the system must stabilize power transmission regardless of PV volatility.

The proposed leg-shared system addresses this mismatch by utilizing the EDLC integrated into the DC bus as a power buffer. To verify the system's ability to maintain stable DWPT operation under fluctuating PV output, the following sections describe a bench-scale evaluation conducted at approximately 1/500 of the actual scale.

D. CONFIGURATION OF SCALED-DOWN MODEL AND EVALUATION METHODOLOGY

For the experimental verification, actual solar irradiance data measured near the Ebina Junction—the target area of this study—is utilized, as shown in Fig. 7. Two distinct scenarios are selected: Day 1, representing stable irradiance for consistent power generation, and Day 2, characterized by severe fluctuations.

Given the massive scale of the real-world power demand, the evaluation is performed using a scaled-down model that maintains the fundamental characteristics of the proposed architecture. Specifically, the received power per vehicle is scaled to approximately 10 W, as derived from the 5.65 kW requirement established in the previous subsection.

Furthermore, due to equipment and time constraints, the 24-hour irradiance profile is compressed into 70 s for the bench-scale experiments. This significant time compression results in a rate of change in solar intensity that is far higher than in actual environmental conditions. Consequently, MPPT control is required to track fluctuations at a much higher speed than in real-time, creating a rigorous testing environment. By maintaining the temporal profile of the irradiance while accelerating its dynamics, this methodology allows for a stringent evaluation of the control system's robustness and the overall effectiveness of the proposed configuration.

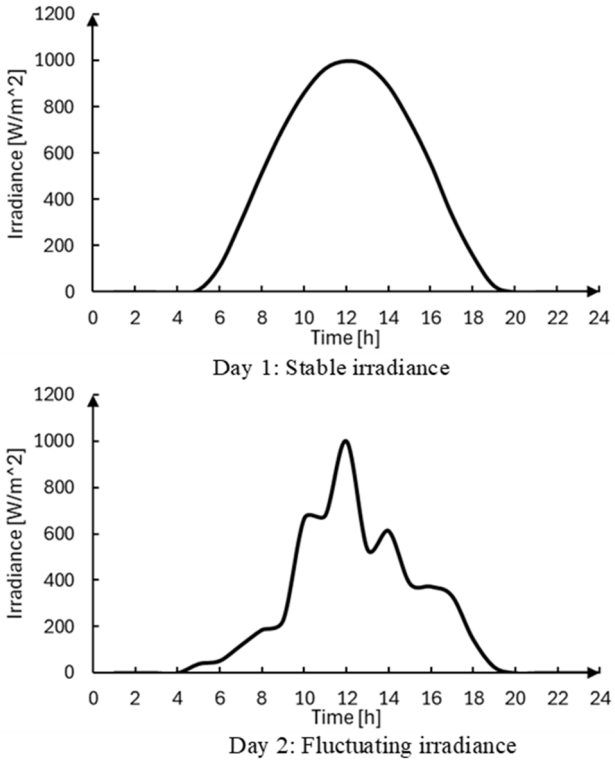

FIGURE 7. The solar irradiance profiles for a stable clear-sky day (Day 1) and a day with severe fluctuations (Day 2).

In the following section, we will describe the conditions and results of bench-scale experiments based on these conditions, along with our analysis.

IV. BENCH-SCALE VERIFICATION OF THE PROPOSED PV+DWPT SYSTEM

A. EXPERIMENTAL SETUP AND PERFORMANCE EVALUATION

This section presents the bench-scale experiment constructed to verify the effectiveness of the proposed system. The circuit configuration and the specific hardware parameters are provided in Fig. 8 and Table 3, respectively.

To evaluate the fundamental operating principles, the experimental setup uses a one-to-one topology with a single transmitting–receiving coil pair. As defined in the control logic, the shared legs switch functionality based on the operational mode. Specifically, the 1st leg operates as a DC–DC boost converter for MPPT during Mode 0, while both the 1st and 2nd legs function as a full-bridge inverter for DWPT during Mode 1. For this prototype, the receiver-side configuration is simplified by modeling the onboard DC–DC

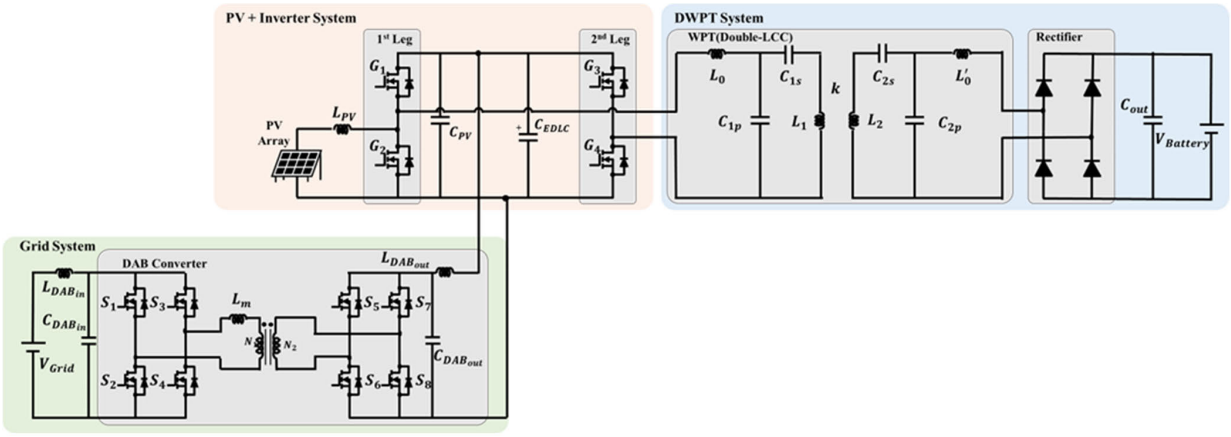

FIGURE 8. Schematic of the proposed system, showcasing the connection between the PV array, the grid-connected DAB converter, and the Double-LCC topology in DWPT. The diagram highlights the proposed leg-shared architecture and the implementation of an EDLC as a DC bus buffer to ensure stable power delivery under dynamic conditions.

TABLE 3. Experiment parameters.

Parameter			Value
PV + Inverter System	L_{PV}	Inductance	0.2mH
	C_{PV}	Capacitance	0.2mF
EDLC	C_{EDLC}	Capacitance	167mF
	$V_{EDLCref}$	Target voltage	40V
Grid System	V_{Grid}	Voltage	30V
	$L_{DAB_{in}}$	Inductance	0.2mH
	$C_{DAB_{in}}$	Capacitance	0.02mF
	L_m	Inductance	0.06mH
	$L_{DAB_{out}}$	Inductance	0.2mH
	$C_{DAB_{out}}$	Capacitance	0.02mF
DWPT System	Tx1 L_o	Inductance	53.6μH
	Tx1 C_{1p}	Capacitance	65.4nF
	Tx1 C_{1s}	Capacitance	22.9nF
	Tx1 L_1	Inductance	206.9μH
	Tx2 L_o	Inductance	49.8μH
	Tx2 C_{1p}	Capacitance	70.4nF
	Tx2 C_{1s}	Capacitance	22.3nF
	Tx2 L_1	Inductance	206.7μH
	Tx3 L_o	Inductance	49.6μH
	Tx3 C_{1p}	Capacitance	70.8nF
	Tx3 C_{1s}	Capacitance	22.3nF
	Tx3 L_1	Inductance	206.4μH
	Rx L_2	Inductance	111.4μH
	Rx C_{2p}	Capacitance	71.2nF
	Rx C_{2s}	Capacitance	56.4nF
	Rx L'_o	Inductance	49.2μH
	C_{out}	Capacitance	0.5mF
	$V_{Battery}$	Voltage	40V

converter and battery as a constant-voltage source to focus on the stability of power delivery from the primary side.

B. EXPERIMENTAL PARAMETERS AND HARDWARE SETUP

To evaluate the dynamic performance of the proposed system, the bench-scale setup was designed to replicate a moving vehicle scenario. As illustrated in the overall view of the system in Fig. 9 and the schematic diagram in Fig. 10, the apparatus consists of a series array of three transmitting coils (Tx_1, Tx_2, and Tx_3) and a single receiving coil (Rx) that traverses the array. The physical dimensions of the coils follow the laboratory's standard specifications: 500×250 mm for the transmitting coil and 250 × 250 mm for the receiving coil, with a covering ratio of 50%. The coupling coefficient between the coils varies dynamically during movement, as plotted in Fig. 11.

In this experiment, the Rx coil travels at a constant speed of 7.2 km/h. Based on the geometric scaling of the coils, this speed corresponds to a real-world velocity of approximately 18.7 km/h. Under these conditions, the Rx coil passes over each transmitting coil in only 0.25 s, requiring the control system to perform mode transitions and tracking within an extremely short timeframe. Furthermore, the setup models a high-density traffic environment equivalent to 60 to 70 vehicles per kilometer. This high-occupancy scenario allows for a rigorous verification of the system's responsiveness to frequent and dynamic power demands.

The experimental evaluation utilizes the solar irradiance profiles previously introduced in Fig. 7 (Day 1: Stable, Day 2: Fluctuating) as the PV input. By applying these real-world fluctuations to the bench-scale model, the robustness of the proposed control algorithm and the buffering effect of the EDLC are thoroughly assessed.

C. EXPERIMENTAL RESULTS (DAY 1)

For clarity in interpreting the experimental waveforms, the schematic diagram of the proposed system is re-illustrated in Fig. 12. The definitions of the variables used in the evaluation are as follows:

- P_{PV}: Output power from the PV
- η_{MPPT}: MPPT efficiency

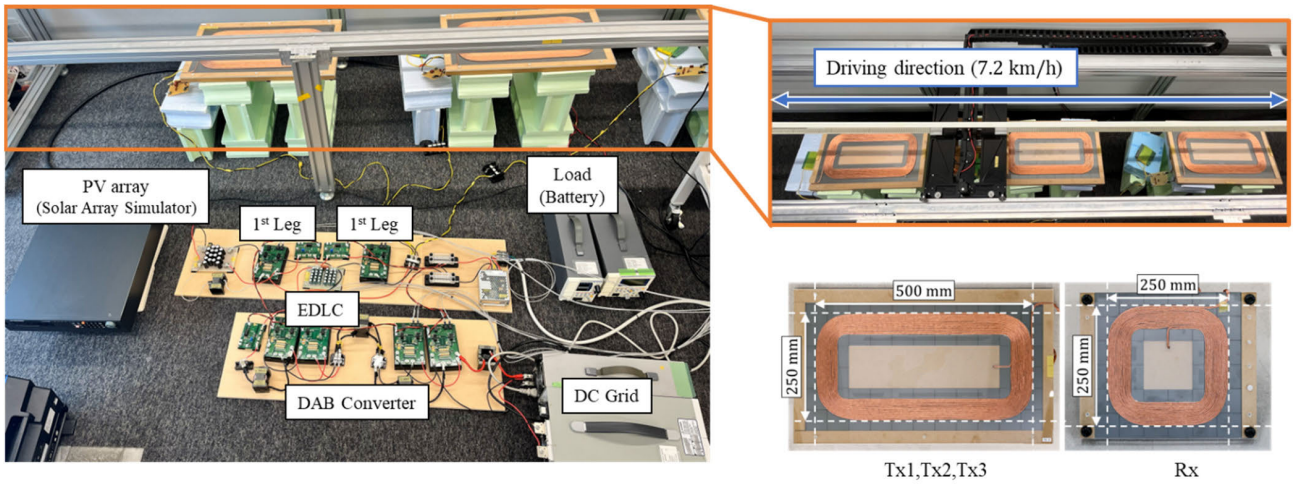

FIGURE 9. The bench-scale experimental apparatus highlights the hardware integration of the solar array simulator, the shared-leg power converter, and the DWPT mechanical setup.

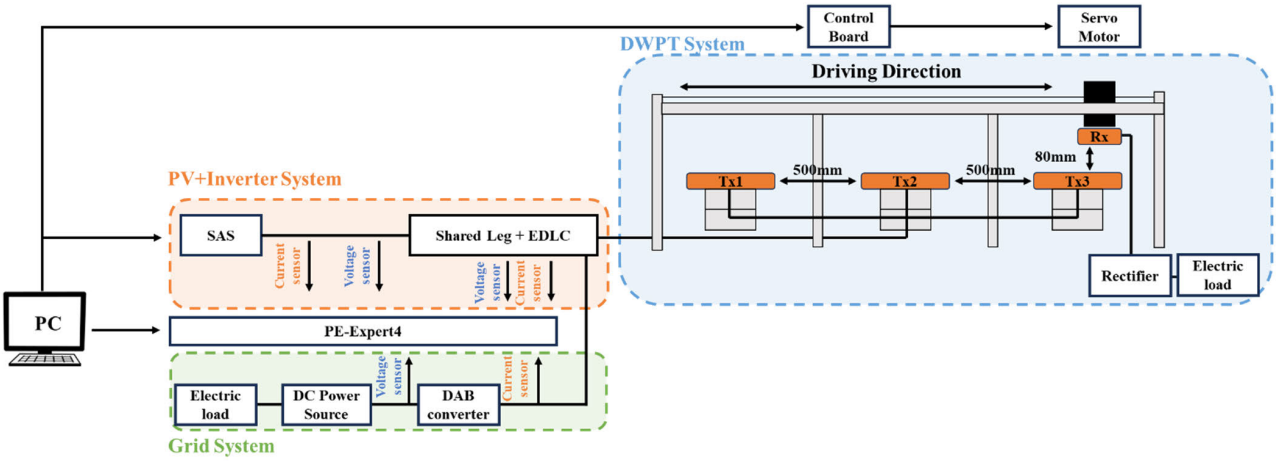

FIGURE 10. A block diagram detailing the integration between the control PC (PE-Expert4), the power conversion stages, and the mechanical DWPT apparatus.

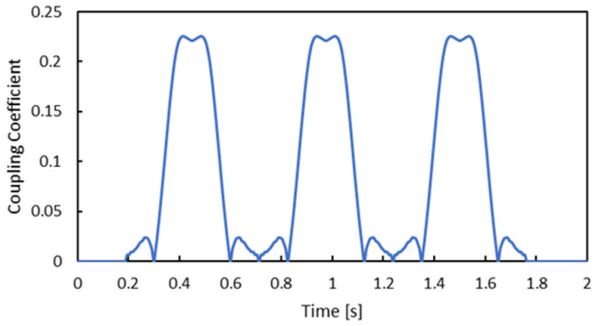

FIGURE 11. Coupling coefficient *k*.

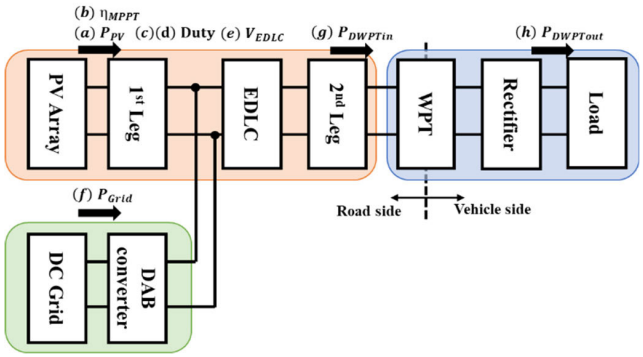

FIGURE 12. Re-illustrated schematic diagram of the proposed system.

- V_{EDLC}: Voltage across the EDLC
- P_{Grid}: Output power from the power grid
- P_{DWPTin}: Power transmitted from the inverter
- $P_{DWPTout}$: Power consumed by the load
- η_{DWPT}: Power transmission efficiency of the DWPT system

The switching frequencies are configured at $f_{Leg} = 85$ kHz for the leg-shared stage and $f_{DAB} = 50$ kH z for the DAB converter.

Fig. 13 presents the bench-scale experimental results for Day 1, which represents the stable solar radiation scenario.

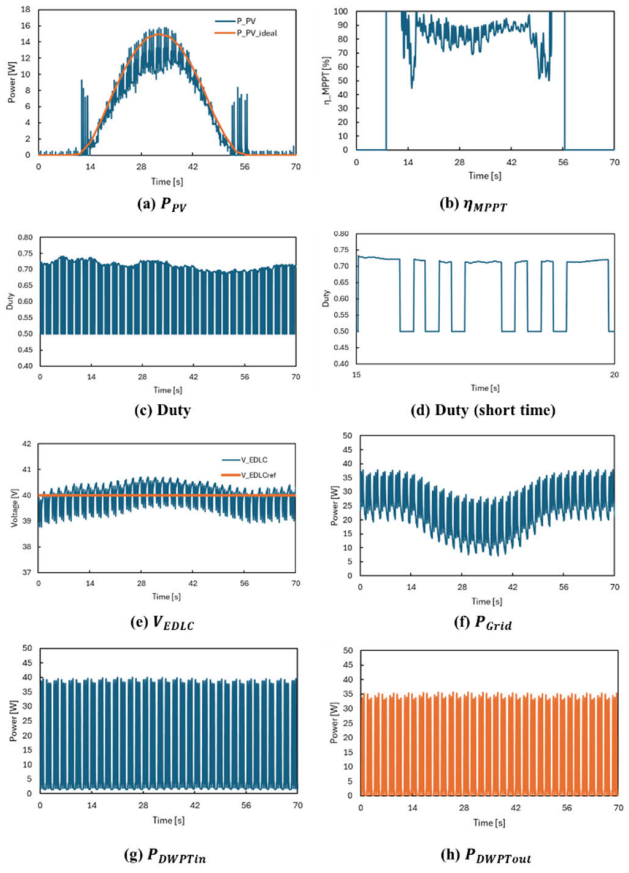

FIGURE 13. Bench-scale experiment results for Day 1.

First, as shown in Fig. 13(a), the PV output power successfully tracks the maximum power point in response to the simulated irradiance profile. Although transient power spikes are observed at approximately 14 s and 56 s, attributed to rapid irradiance changes and circuit interference inherent in high-frequency operation 85 kHz, the system demonstrates rapid convergence to a steady state, maintaining an average MPPT efficiency of 78.5% even under accelerated time-scale conditions shown on Fig. 13(b).

The core functionality of the leg-shared section is validated in Figs. 13(c) and (d), where the duty ratio transitions instantaneously from its MPPT-controlled fluctuations to the optimal fixed value of 0.5 during vehicle passage. This seamless switch between converter and inverter operations within a single set of legs confirms the algorithm's ability to prioritize DWPT while maximizing hardware utilization. Regarding the EDLC's role as a power buffer, Fig. 13(e) shows that the voltage is controlled with exceptional precision, exhibiting an average error of only 0.84% relative to the target, with the peak error limited to 3.72% during transients. This stability is reflected in the grid power behavior shown in Fig. 13(f); while P_{Grid} exhibits periodic fluctuations due to the DWPT-priority control, the EDLC effectively absorbs both PV volatility and abrupt load shifts, thereby mitigating direct power spikes to the grid.

Finally, as shown in Figs. 13(g) and (h), the system achieved an average transmitted power of 13.06 W and an average received power of 10.06 W, resulting in a transmission efficiency of 81.2%. These results prove that the proposed system consistently fulfills the design goal of a stable 10 W power supply in a simulated real-world environment while maintaining a simplified circuit architecture.

D. EXPERIMENTAL RESULTS (DAY 2)

Fig. 14 presents the bench-scale experimental results for Day 2, which features volatile solar irradiance conditions caused by simulated cloud cover.

First, examining the PV response in Fig. 14(a) reveals that the proposed system's MPPT control rapidly adapts to abrupt irradiance changes. While transient spikes similar to those in the stable scenario are observed, they represent the inherent physical response to stochastic disturbances under the accelerated time scale. Notably, the MPPT efficiency under these volatile conditions reached 85.2% shown in Fig. 14(b), exceeding the results from Day 1. This confirms that the leg-shared converter maintains high dynamic responsiveness and tracking accuracy even under severe irradiance fluctuations.

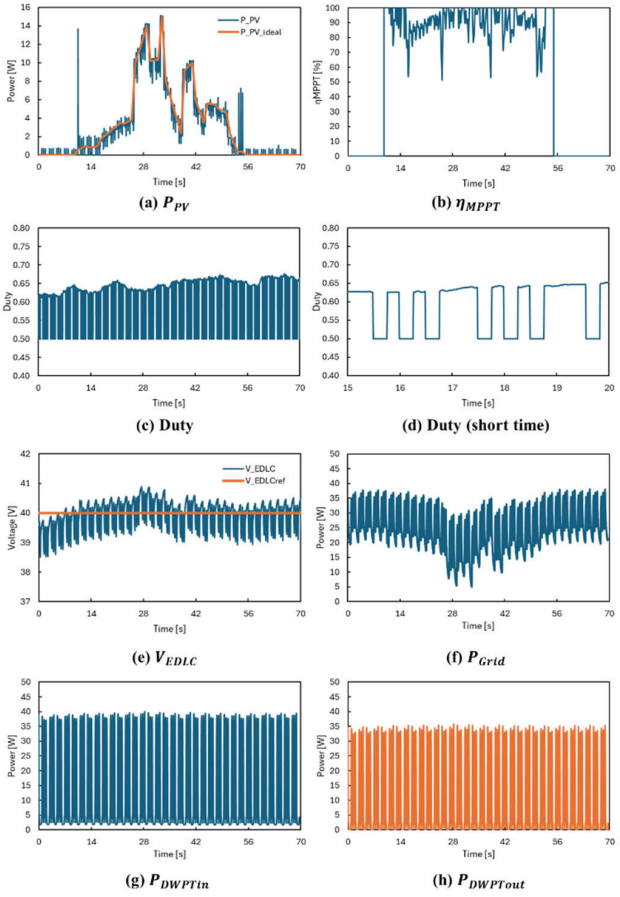

FIGURE 14. Bench-scale experiment results for Day 2.

The behavior of the leg-shared section is further illustrated in Figs. 14(c) and (d). To accommodate the shifting

PV output, the duty ratio undergoes frequent and significant adjustments during MPPT operation. However, at the moment of vehicle passage, the control precisely transitions to the fixed value of 0.5, mirroring the stability observed on Day 1. The fact that the DWPT inverter operation remains unaffected by intense irradiance volatility underscores the robustness and high responsiveness of the proposed switching algorithm.

Regarding system stability, Fig. 14(e) shows that the V_{EDLC} average tracking error remains within 0.93%, with the with the peak error limited to 3.73%, maintaining exceptional stability comparable to the stable irradiance scenario. This precise voltage regulation prevents sharp PV fluctuations from propagating to the DWPT load or the utility grid. Consequently, as shown in Fig. 14(f), the EDLC appropriately counteracts the variations in solar generation, effectively suppressing abrupt grid power fluctuations and mitigating the burden on the external power source.

Finally, the DWPT performance is summarized in Figs. 14(g) and (h). The average transmitted power was 13.35 W, and the average received power was 10.70 W, resulting in a transmission efficiency of 80.2%. This performance is nearly equivalent to the 81.2% achieved on Day 1, proving that the system reliably fulfills the design target of a stable 10 W received power regardless of weather conditions. These results validate the effectiveness of the proposed leg-shared DWPT system as a robust power supply infrastructure that ensures consistent energy delivery through intelligent power buffering and mode-switching control.

E. DISCUSSION ON STABILITY AND PRACTICAL SCALABILITY

The experimental results for both Day 1 and Day 2 scenarios demonstrate the robustness of the proposed system.

Although the solar irradiance profiles differed significantly, the coordinated control effectively managed the power flow in both cases. Specifically, while Day 1 showed smoother transitions, the maximum voltage deviation occurred during the aggressive fluctuations of Day 2, where it was suppressed within 0.93% of the rated voltage.

This stability under disparate weather conditions provides quantitative evidence of the grid-impact mitigation. Since the EDLC-based buffer absorbed the high-frequency power spikes, the power grid was effectively shielded from these transients. Regarding the scalability, although the current validation was conducted at a 10 W bench-scale, the underlying principles of the leg-shared architecture and the integrated control laws are not limited by power capacity. In practical kW-class infrastructure, high-power semiconductors (e.g., SiC or GMOSFETs) and their associated cooling systems are the primary drivers of system cost and volume. Therefore, the 33.3% reduction in switching elements achieved by the proposed leg-sharing topology becomes even more significant at scale, leading to a direct reduction in hardware footprint and material costs.

Additionally, from the perspective of efficiency and thermal management, reducing the number of power devices inherently minimizes the sources of conduction and switching losses. This simplicity simplifies the thermal design of heat sinks in high-power applications. By scaling the semiconductor ratings and passive component values based on standard power electronics design principles, the proposed system can be implemented in kW-class practical infrastructure while maintaining high efficiency.

Moreover, the achieved DC bus stability within 0.93% is a normalized performance indicator; since the control strategy manages power mismatch ratios rather than absolute values, these results serve as a reliable proxy for high-power performance.

The validity of these results is further reinforced by the aggressive time compression (70 s vs. 24 h). By compressing the daily solar cycle into a very short duration, the control system was subjected to power fluctuations that are much more rapid and extreme than those encountered in real-time environments. Success under these stringent conditions confirms that the control bandwidth is sufficiently wide to track aggressive transients. Because practical real-time dynamics are much slower, the required control sampling rates and response times remain well within the capabilities of standard industrial controllers. This demonstrates a high safety margin, suggesting that the proposed integrated control can reliably manage the relatively slower dynamics of practical kW-class infrastructure.

V. CONCLUSION

This study has presented a novel integrated architecture for PV generation and DWPT to facilitate carbon neutrality and extend the cruising range of EVs. The proposed system addresses the challenges of low hardware utilization and grid instability. The system integrates the PV boost DC–DC converter and the DWPT full-bridge inverter using a leg-shared configuration. This architecture reduces the switching element by 33.3%, contributing to significant circuit simplification and equipment miniaturization. Furthermore, the integration of an EDLC-based power buffer effectively smooths the stochastic fluctuations of PV output and the intermittent power demands of DWPT.

The effectiveness of the proposed system was validated through bench-scale experiments. The results confirmed that the system maintains a high MPPT efficiency, reaching an average of 85.2%, even under rigorous time-scale fluctuations. Additionally, the DWPT transmission efficiency exceeded 80%, successfully delivering a stable power supply of 10 W. Regarding grid interaction, the EDLC successfully absorbed abrupt power spikes. It ensured DC bus stability within 0.93% of the rated voltage, providing quantitative evidence of grid-impact mitigation.

In summary, the proposed system demonstrates a robust capability to provide a stable power supply and reduce grid impacts while remaining resilient to weather conditions and load variations. Future research will focus on further enhancing MPPT efficiency through variable step-width or incremental conductance methods and improving control tracking performance for high-speed highway scenarios (exceeding 80 km/h). Furthermore, by scaling the prototype to real-world power levels and developing coordinated control algorithms for multi-vehicle scenarios, the practicality of this system for widespread societal implementation will be further advanced.

REFERENCES

[1] Y. Yamada, K. Sasaki, T. Imura, and Y. Hori, "Design method of coils for dynamic wireless power transfer considering average transmission power and installation rate," in *Proc. IEEE Southern Power Electron. Conf. (SPEC)*, Dec. 2021, pp. 1–8.

[2] K. Hanawa, T. Imura, and N. Abe, "Basic evaluation of electrical characteristics of ferrite-less and capacitor-less coils by road embedment experiment for dynamic wireless power transfer," in *Proc. IEEE PELS Workshop Emerg. Technol., Wireless Power Transf. (WoW)*, Jun. 2021, pp. 1–5.

[3] A. C. Bagchi, A. Kamineni, R. A. Zane, and R. Carlson, "Review and comparative analysis of topologies and control methods in dynamic wireless charging of electric vehicles," *IEEE J. Emerg. Sel. Topics Power Electron.*, vol. 9, no. 4, pp. 4947–4962, Aug. 2021.

[4] C. H. Lee, G. Jung, K. A. Hosani, B. Song, D.-K. Seo, and D. Cho, "Wireless power transfer system for an autonomous electric vehicle," in *Proc. IEEE Wireless Power Transf. Conf. (WPTC)*, Nov. 2020, pp. 467–470.

[5] Y. Yamada, T. Imura, and Y. Hori, "A method for determining resonant elements considering the requirements of double-LCC circuits in dynamic wireless power transfer," in *Proc. Wireless Power Week (WPW)*, Bordeaux, France, Jul. 2022, pp. 766–771.

[6] B. Pakhaliuk, O. Husev, V. Shevchenko, K. Kroics, D. Stepins, and R. Strzelecki, "Automatic position detection and transmitting activation of dynamic wireless power transfer system with air capacitor," in *Proc. Wireless Power Week (WPW)*, Bordeaux, France, Jul. 2022, pp. 487–491.

[7] D. Patil, M. K. McDonough, J. M. Miller, B. Fahimi, and P. T. Balsara, "Wireless power transfer for vehicular applications: Overview and challenges," *IEEE Trans. Transport. Electrific.*, vol. 4, no. 1, pp. 3–37, Mar. 2018.

[8] H. Feng, T. Cai, S. Duan, J. Zhao, X. Zhang, and C. Chen, "An LCC-compensated resonant converter optimized for robust reaction to large coupling variation in dynamic wireless power transfer," *IEEE Trans. Ind. Electron.*, vol. 63, no. 10, pp. 6591–6601, Oct. 2016.

[9] R. Tavakoli and Z. Pantic, "Analysis, design, and demonstration of a 25-kW dynamic wireless charging system for roadway electric vehicles," *IEEE J. Emerg. Sel. Topics Power Electron.*, vol. 6, no. 3, pp. 1378–1393, Sep. 2018.

[10] K. Hanawa, T. Imura, Y. Hori, and N. Abe, "Proposal of coil embedment method by pouring resin materials for dynamic wireless power transfer," in *Proc. Wireless Power Week (WPW)*, Bordeaux, France, Jul. 2022, pp. 761–765.

[11] C. Cui, K. Song, C. Zhu, Q. Zhang, Y. Liu, and S. Dong, "State feedback controller design of dynamic wireless power transfer system," in *Proc. IEEE PELS Workshop Emerg. Technol., Wireless Power Transf. (Wow)*, Montreal, QC, Canada. Union City, NJ, USA: Wire, Jun. 2018, pp. 1–5.

[12] K. Kumar, K. V. V. S. R. Chowdary, P. Sanjeevikumar, and R. Prasad, "Analysis of solar PV fed dynamic wireless charging system for electric vehicles," in *Proc. IECON 47th Annu. Conf. IEEE Ind. Electron. Soc.*, Oct. 2021, pp. 1–6.

[13] T. Theodoropoulos, A. Amditis, J. Sallán, H. Bludszuweit, B. Berseneff, P. Guglielmi, and F. Deflorio, "Impact of dynamic EV wireless charging on the grid," in *Proc. IEEE Int. Electr. Vehicle Conf. (IEVC)*, Dec. 2014, pp. 1–7.

[14] R. Zeng, V. Galigekere, O. Onar, and B. Ozpineci, "Optimized renewable energy integration for EV high-power dynamic wireless charging systems," in *Proc. IEEE Power Energy Soc. Innov. Smart Grid Technol. Conf. (ISGT)*, Feb. 2021, pp. 1–5.

[15] T. M. Newbolt, P. Mandal, H. Wang, and R. Zane, "Diverse effects of dynamic wireless power transfer roadway in-motion electric vehicle charging," in *Proc. IEEE Power Energy Soc. Innov. Smart Grid Technol. Conf. (ISGT)*, Washington, DC, USA, Jan. 2023, pp. 1–5.

[16] M. Sugizaki, S. Urano, T. Imura, and Y. Hori, "Proposal for the system of dynamic wireless power transfer connected with photovoltaic in the off-grid environment," in *Proc. IEEE 7th Southern Power Electron. Conf. (SPEC)*, Nadi, Fiji, Dec. 2022, pp. 1–6.

[17] N. Murayama, T. Imura, and Y. Hori, "Power stabilization of dynamic wireless power transfer system with grid-connected photovoltaic and DC bus voltage control," in *Proc. IEEE Wireless Power Technol. Conf. Expo. (WPTCE)*, May 2024, pp. 205–208.

[18] S. Urano, M. Sugizaki, T. Imura, and Y. Hori, "Basic experiment on the integration of grid-connected photovoltaic and dynamic wireless power transfer," in *Proc. IEEE 7th Southern Power Electron. Conf. (SPEC)*, Nadi, Nadi, Fiji, Dec. 2022, pp. 1–6.

[19] N. Murayama, T. Imura, and Y. Hori, "Bench-scale experiment of dynamic wireless power transfer system with grid-connected photovoltaic and DC bus voltage control," in *Proc. IEEE Wireless Power Technol. Conf. Expo. (WPTCE)*, Rome, Italy, Jun. 2025, pp. 1–5.

[20] X. Liu and L. A. C. Lopes, "An improved perturbation and observation maximum power point tracking algorithm for PV arrays," in *Proc. IEEE 35th Annu. Power Electron. Spec. Conf.*, Aachen, Germany, 2004, pp. 2005–2010.

[21] J. Zhou, "Simulation research on maximum power point tracking based on perturbation and observation," in *Proc. 10th World Congr. Intell. Control Autom.*, Beijing, China, Jul. 2012, pp. 150–153.

[22] D. K. Sharma and G. Purohit, "Advanced perturbation and observation (P&O) based maximum power point tracking (MPPT) of a solar photovoltaic system," in *Proc. IEEE 5th India Int. Conf. Power Electron. (IICPE)*, Delhi, India, Dec. 2012, pp. 1–5.

[23] K. Sasaki and T. Imura, "Combination of sensorless energized section switching system and double-LCC for DWPT," in *Proc. IEEE PELS Workshop Emerg. Technol., Wireless Power Transf. (WoW)*. Union City, NJ, USA: Wire, Nov. 2020, pp. 62–67.

[24] X. Zhang, J. Wang, M. Xue, Y. Li, and Q. Yang, "Reserch on dynamic wireless charging of electric vehicle based on double LCC compensation mode," in *Proc. IEEE Wireless Power Transf. Conf. (WPTC)*, Jun. 2019, pp. 141–145.

[25] H.-R. Cha, K.-H. Park, Y.-J. Choi, and R.-Y. Kim, "Double-sided LCC compensation topology with semi-bridgeless rectifier for wireless power transfer system," in *Proc. 10th Int. Conf. Power Electron. ECCE Asia (ICPE-ECCE Asia)*, May 2019, pp. 1–6.

[26] L. Peng, L. Xiao-Kun, G.-R. Zhu, M. Xie, Li, and Xiao-Song, "Characteristics research on double LCC compensation converter in the inductive energy transfer system," in *Proc. Int. Conf. Ind. Informat. Comput. Technol., Intell. Technol., Ind. Inf. Integr.*, Wuhan, China, Dec. 2015, pp. 243–246.

[27] Z. Shan, J. Jatskevich, H. H.-C. Iu, and T. Fernando, "Simplified load-feedforward control design for dual-active-bridge converters with current-mode modulation," *IEEE J. Emerg. Sel. Topics Power Electron.*, vol. 6, no. 4, pp. 2073–2085, Dec. 2018.

[28] New Energy and Industrial Technology Development Organization (NEDO). *Solar Radiation Database Monitoring System (METPV-20): Annual Hourly Solar Radiation Database*. [Online]. Available: https://appww2.infoc.nedo.go.jp/appww/metpv.html?p=46091

[29] Ministry of Land, Infrastructure, Transport and Tourism (MLIT). (2021). *2021 Road Traffic Census Visualization Tool: General Traffic Volume Survey Results*. [Online]. Available: https://www.mlit.go.jp/road/ir/ir-data/census_visualizationR3/index.html

[30] Nissan Motor Co., Ltd. *Nissan LEAF (62-kWh Model) Charging Specifications*. Nissan Motor Co. [Online]. Available: https://history.nissan.co.jp/LEAF/ZE1/1901/charge.html

NOZOMI MURAYAMA (Student Member, IEEE) received the degree from the Department of Electrical Engineering, Faculty of Science and Technology, Tokyo University of Science, in March 2024. She is currently pursuing the degree with the Department of Electrical Engineering, Graduate School of Science and Technology, Tokyo University of Science. She is focusing on the realization of a system that combines photovoltaic and dynamic wireless power transfer.

TAKEHIRO IMURA (Member, IEEE) received the bachelor's degree in electrical and electronics engineering from Sophia University, Tokyo, Japan, in 2005, and the M.E. degree in electronic engineering and the D.Eng. degree in electrical engineering from The University of Tokyo, Tokyo, in 2007 and 2010, respectively. He joined the Department of Advanced Energy, Graduate School of Frontier Sciences, The University of Tokyo, as a Research Associate, where he has been a Project Lecturer, since 2015. In 2019, he joined the Department of Electrical Engineering, Tokyo University of Science, as an Associate Professor. He is currently investigating wireless power transfer using magnetic resonant coupling and electric resonant coupling. His research interests include electric vehicle in-motion connected to renewable energy, sensors, and cancer treatment. He is a member of the Institute of Electronics, Information and Communication Engineers (IEICE) and the Society of Automotive Engineers of Japan (JSAE). He is the Winner of the IEEJ Industry Applications Society Distinguished Transaction Paper Award, in 2015, and the IEEE Power Electronics Transactions First Prize Paper Award, in 2017.

YOICHI HORI received the B.S., M.S., and Ph.D. degrees in electrical engineering from The University of Tokyo, Tokyo, Japan, in 1978, 1980, and 1983, respectively. In 1983, he joined the Department of Electrical Engineering, The University of Tokyo, as a Research Associate. Later, he became an Assistant Professor, an Associate Professor, and a Professor at The University of Tokyo, in 2000. In 2002, he moved to the Information and System Division, Institute of Industrial Science, as a Professor. In 2002, he moved to the Information and System Division, Institute of Industrial Science, as a Professor. In 2008, he moved to the Department of Advanced Energy, Graduate School of Frontier Sciences, The University of Tokyo. He retired in March 2021 and has been with Tokyo University of Science, since April 2021. He was a Professor Emeritus with The University of Tokyo. From 1991 to 1992, he was a Visiting Researcher at the University of California at Berkeley. Recently, he has also been focusing on the research and promotion of wireless power transfer. His research interests include control theory and its industrial applications to motion control, mechatronics, robotics, and electric vehicles. He is a Past AdCom Member of the Industrial Electronics Society (IES). He is currently a Fellow Member of the Institute of Electrical Engineers of Japan (IEEJ), the Society of Automotive Engineers of Japan (JSAE), Japan Society of Simulation Technology (JSST), and several other organizations. He is the Winner of the Best Transactions Paper Award from the IEEE TRANSACTIONS ON INDUSTRIAL ELECTRONICS, in 1993, 2001, and 2013; the 2000 Best Transactions Paper Award from IEEJ; and the 2011 Achievement Award of IEEJ. He was the President of the Industry Applications Society of IEEJ and World Electric Vehicle Association (WEVA), the Director of Japan Automobile Research Institute (JARI), and the Vice-President of JSAE. He is the President of Capacitors Forum, the Chairman of the Motor Technology Symposium of Japan Management Association (JMA), and the Representative Director of the Next Generation Vehicle Promotion Center (NeV). He has been the Treasurer of the IEEE Japan Council and Tokyo Section in a few years, since 2001.